Methyl B_{12} Models Containing Unsubstituted Imidazole As an Axial Ligand Investigated by Structural and NMR Spectroscopic Methods. Evidence that μ-Imidazolato-Bridged Dimers Are Formed by Base Addition to Some Analogues with Macrocyclic Equatorial Ligands Incorporating BF_2

Scott J. Moore,[†] Alexander Kutikov,[†] Rene J. Lachicotte,[‡] and Luigi G. Marzilli*[,†]

Department of Chemistry, Emory University, Atlanta, Georgia 30322 and Department of Chemistry, University of Rochester, Rochester, New York 14627

Received August 11, 1998

Imidazole (imH)-containing B_{12} model complexes that could possibly be deprotonated at the imidazole NH to form the corresponding imidazolato (im) complexes were investigated. Organomethyl complexes of cobaloxime and imine/oxime (I/O) analogues with equatorial ligands possessing an O−BF_2−O moiety in place of each deprotonatable O−H- - -O moiety of standard models were prepared. In some cases, NMR spectroscopy revealed formation of μ-imidazolato (μ-im) dimers in methanol-d_4 on addition of methoxide. The desired monomeric imidazolato species was not formed at a characterizable level. We present the X-ray crystal structures of LCo(DBF_2)$_2$$CH_3$ (where L = imH, 4-*t*-BuimH) and [$AsPh_4$][(μ-im)(Co(DBF_2)$_2$$CH_3$)$_2$] ($DBF_2$ = the BF_2-substituted monoanion of dimethylglyoxime). The latter confirms the NMR solution studies and is the first structure of a B_{12} model species bridged by an imidazolato moiety. We have also structurally characterized the related I/O complexes, [imHCo((DO)($DOBF_2$)pn)CH_3]PF_6 and [imHCo((DO)(DOH)pn)CH_3]I. The former is the first reported I/O structure with a BF_2 bridge. The structures presented here greatly increase the data available for B_{12} model derivatives with imidazole NH groups and nearly double the number of reported structures for the LCo(DBF_2)$_2$$CH_3$ type of B_{12} models. As in all previous BF_2-containing models, the equatorial moieties adopt the extended chair conformation. For the LCo(DBF_2)$_2$$CH_3$ (L = imH, 4-*t*-BuimH) compounds, this arrangement leads to an L orientation that is unusual. Normally, the L plane bisects either the six-membered or the five-membered equatorial chelate rings (A and B orientations, respectively). The L orientation we find is intermediate between the typical A- and the B-type L orientations. Compared to that in A-type imHCo(DH_2)$_2$$CH_3$ (DH = monoanion of dimethylglyoxime), the Co−N_L distance for imHCo(DBF_2)$_2$$CH_3$ was longer. We attribute this lengthening to the intermediate A-/B-type orientation. However, the distance shortens upon formation of the imidazolato dimer. The relationship of the μ-im ligand to both Co(DBF_2)$_2$$CH_3$ moieties is also intermediate A/B and hence unusual. Therefore, this shortening probably does not have a steric cause but results from the better electron-donor ability of the imidazolato ligand. Measurements of $^1J_{CH}$ of Co−CH_3 are consistent with this conclusion.

Introduction

The recent crystal structures of methylcobalamin (MeB_{12})-dependent methionine synthase[1] and adenosylcobalamin-dependent methylmalonyl-coenzyme A mutase[2] have revealed the coordination of a histidine imidazole ring in the site occupied by the tethered dimethylbenzimidazole in the unbound cofactor. This imidazole links the cofactor with the other members of the functional unit known as the catalytic quartet. The hydrogen bonding network of the catalytic quartet, involving the imidazole ring NH, is hypothesized to enhance electron donation from an incipient monodentate imidazolato ligand to cobalt; such modulation of the electronic nature of the cobalt center mediated by the protein may be a significant component in catalysis.[1−3]

We recently investigated the effect in solution of binding imidazole to methylcobinamide in aqueous solution.[3] More precise information about the effect of NH hydrogen bonding or even NH deprotonation can be obtained from simple models.[3,4] Such simple models would allow the role of the corrin ring to be better understood. Unfortunately, very few B_{12} model compounds of an imidazole ligand with an endocyclic NH group have been studied. Since such complexes, especially when the axial ligand L is imidazole (imH), are relatively difficult to dissolve in organic solvents normally used to study models, few have afforded X-ray quality crystals.

The cobaloxime (LCo(DH)$_2$R) and imine/oxime (I/O, [LCo((DO)(DOH)pn)R]$^+$) classes of B_{12} models (Chart 1, X = H) have been well characterized with numerous axial ligands.[5−33]

[†] Emory University.
[‡] University of Rochester.

(1) Drennan, C. L.; Huang, S.; Drummond, J. T.; Matthews, R. G.; Ludwig, M. L. *Science (Washington, D.C.)* **1994**, *266*, 1669.
(2) Mancia, F.; Keep, N. H.; Nakagawa, A.; Leadlay, P. F.; McSweeney, S.; Rasmussen, B.; Bösecke, P.; Diat, O.; Evans, P. R. *Structure* **1996**, *4*, 339.
(3) Puckett, J. M., Jr.; Mitchell, M. B.; Hirota, S.; Marzilli, L. G. *Inorg. Chem.* **1996**, *35*, 4656.
(4) Randaccio, L.; Furlan, M.; Geremia, S.; Slouf, M. *Inorg. Chem.* **1998**, *37*, 5390.
(5) Bresciani-Pahor, N.; Forcolin, M.; Marzilli, L. G.; Randaccio, L.; Summers, M. F.; Toscano, P. J. *Coord. Chem. Rev.* **1985**, *63*, 1.
(6) Randaccio, L.; Bresciani Pahor, N.; Zangrando, E.; Marzilli, L. G. *Chem. Soc. Rev.* **1989**, *18*, 225.
(7) Marzilli, L. G.; Marzilli, P. A. In *Vitamin B_{12} and B_{12}-Proteins*; Kräutler, B., Arigoni, D., Golding, B. T., Eds.; Wiley-VCH: Weinheim, 1998; p 369.

10.1021/ic980944d CCC: $18.00
Published on Web 02/05/1999

Chart 1

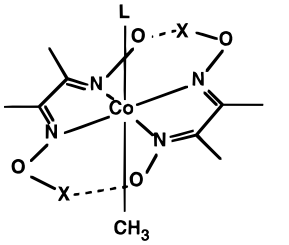

$LCo(DX)_2CH_3$

X = H, BF_2

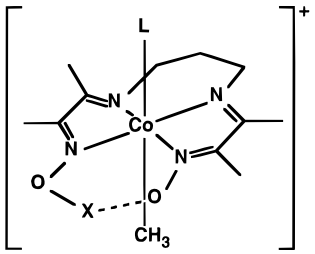

$[LCo((DO)(DOX)pn)CH_3]^+$

X = H, BF_2

Expansion of these organocobalt model systems to include imidazole species with a titratable NH proton would produce compounds that would allow us to probe how an imidazolato ligand induces electronic changes in the trans alkyl group. However, the equatorial moieties of both the cobaloxime and I/O models contain ionizable protons that complicate any attempt to deprotonate a ligand such as imH. For both types of models, close analogues are known with BF_2 moieties in place of the bridging protons,[34,35] including few crystal structures for the cobaloximes.[36−39] The equatorial macrocyclic ligands, $(DBF_2)_2$ and $(DO)(DOBF_2)pn$ (Chart 1, X = BF_2), lack highly reactive protons, and the endocyclic NH of an axially bound imidazole should be the most acidic site in the models. We hoped to generate imidazolato complexes from such precursors. Other types of moieties have been used to replace the bridging protons,[40−42] or other types of oximes have been bridged by BF_2 groups.[38] The aforementioned are selected examples of other alternative compounds that could have been used, but we chose to concentrate on the B_{12} models (Chart 1, X = BF_2) because of the useful database available.

For deprotonation studies, we synthesized and characterized several organocobalt complexes with imidazole NH groups. Although our goal was to convert these to monodentate imidazolato complexes, we observed mainly dimerization to μ-imidazolato complexes in basic methanol-d_4. However, since it must donate to two metal centers, a μ-imidazolato ligand is an even better model of the putative incipient monodentate imidazolato ligand than is the fully deprotonated monodentate imidazolato ligand.

Experimental Section

Materials and Syntheses. $[AsPh_4]Cl\cdot H_2O$ (Strem) and all other reagents (Aldrich) were used without further purification. Acetone-d_6 and methanol-d_4 solvents were from Isotec, Inc. 4-*tert*-Butylimidazole (4-*t*-Bu-imH) was prepared from bromopinacolone[43] by Jönsson's procedure.[44] $pyCo(DH)_2CH_3$ was prepared as previously described.[45,46] Elemental analyses were performed by Atlantic Microlab, Inc. (Atlanta, GA).

$H_2OCo(DBF_2)_2CH_3$ was prepared by modifying the reported method.[34,35] A large excess of $BF_3\cdot Et_2O$ (8.4 mL, 0.067 mol) was added to $pyCo(DH)_2CH_3$ (5.03 g, 0.0131 mol) that was sealed in a flask under N_2. After the suspension was stirred for ~5 min, CH_2Cl_2 (100 mL) and *n*-Bu_3N (not dried, 6 mL in 20 mL CH_2Cl_2) were added in succession. The orange suspension, sonicated for ~10 min to break up large particles, was stirred overnight. The resulting suspended yellow solid was isolated by filtration, washed with H_2O (4 × 15 mL) and dried overnight under vacuum, giving 2.72 g of crude product. Addition of the water filtrates to the CH_2Cl_2 filtrate precipitated a second crop (2.30 g) that was isolated, washed with CH_2Cl_2 (30 mL) and H_2O (20 mL), and dried overnight under vacuum. The ^1H NMR spectra (Tables 1 and 2) agreed with the reported shift values for the aqua complex[47] but indicated traces of protonated *n*-Bu_3N. The absence of peaks in

(8) Marzilli, L. G. In *Bioinorganic Catalysis*, 2nd ed.; Reedijk, J., Bouwman, E., Eds.; Marcel Dekker: New York, 1999.
(9) Nie, S.; Marzilli, L. G.; Yu, N.-T. *J. Am. Chem. Soc.* **1989**, *111*, 9256.
(10) Attia, W. M.; Zangrando, E.; Randaccio, L.; Antolini, L.; López, C. *Acta Crystallogr.* **1989**, *C45*, 1500.
(11) Bresciani-Pahor, N.; Attia, W. M.; Geremia, S.; Randaccio, L.; López, C. *Acta Crystallogr.* **1989**, *C45*, 561.
(12) Charland, J.-P.; Attia, W. M.; Randaccio, L.; Marzilli, L. G. *Organometallics* **1990**, *9*, 1367.
(13) Bresciani-Pahor, N.; Randaccio, L.; Zangrando, E. *Inorg. Chim. Acta* **1990**, *168*, 115.
(14) Toscano, P. J.; Brand, H.; Geremia, S.; Randaccio, L.; Zangrando, E. *Organometallics* **1991**, *10*, 713.
(15) Geremia, S.; Mari, M.; Randaccio, L.; Zangrando, E. *J. Organomet. Chem.* **1991**, *408*, 95.
(16) Gerli, A.; Sabat, M.; Marzilli, L. G. *J. Am. Chem. Soc.* **1992**, *114*, 6711.
(17) Gerli, A.; Marzilli, L. G. *Inorg. Chem.* **1992**, *31*, 1152.
(18) Marzilli, L. G.; Gerli, A.; Calafat, A. M. *Inorg. Chem.* **1992**, *31*, 4617.
(19) Geremia, S.; Randaccio, L.; Zangrando, E.; Antolini, L. *J. Organomet. Chem.* **1992**, *425*, 131.
(20) Charland, J.-P.; Zangrando, E.; Bresciani-Pahor, N.; Randaccio, L.; Marzilli, L. G. *Inorg. Chem.* **1993**, *32*, 4256.
(21) Randaccio, L.; Geremia, S.; Zangrando, E.; Ebert, C. *Inorg. Chem.* **1994**, *33*, 4641.
(22) Geremia, S.; Dreos, R.; Randaccio, L.; Tauzher, G.; Antolini, L. *Inorg. Chim. Acta* **1994**, *216*, 125.
(23) Hirota, S.; Polson, S. M.; Puckett, J. M., Jr.; Moore, S. J.; Mitchell, M. B.; Marzilli, L. G. *Inorg. Chem.* **1996**, *35*, 5646.
(24) Polson, S. M.; Hansen, L.; Marzilli, L. G. *J. Am. Chem. Soc.* **1996**, *118*, 4804.
(25) Polson, S. M.; Cini, R.; Pifferi, C.; Marzilli, L. G. *Inorg. Chem.* **1997**, *36*, 314.
(26) Polson, S. M.; Hansen, L.; Marzilli, L. G. *Inorg. Chem.* **1997**, *36*, 307.
(27) Marzilli, L. G.; Polson, S. M.; Hansen, L.; Moore, S. J.; Marzilli, P. A. *Inorg. Chem.* **1997**, *36*, 3854.
(28) Randaccio, L.; Geremia, S. *Organometallics* **1997**, *16*, 4951.
(29) Moore, S. J.; Iwamoto, M.; Marzilli, L. G. *Inorg. Chem.* **1998**, *37*, 1169.
(30) Moore, S. J.; Lachicotte, R. J.; Sullivan, S. T.; Marzilli, L. G. *Inorg. Chem.* **1999**, *38*, 383−390.
(31) Moore, S. J.; Marzilli, L. G. *Inorg. Chem.* **1998**, *37*, 5329.
(32) Hirota, S.; Kosugi, E.; Marzilli, L. G.; Yamauchi, O. *Inorg. Chim. Acta* **1998**, *275*−*276*, 90.
(33) Cini, R.; Moore, S. J.; Marzilli, L. G. *Inorg. Chem.* **1998**, *37*, 6890.
(34) Schrauzer, G. N.; Windgassen, R. J. *J. Am. Chem. Soc.* **1966**, *88*, 3738.
(35) Cartano, A. V.; Ingraham, L. L. *Bioinorg. Chem.* **1977**, *7*, 351.
(36) Ram, M. S.; Riordan, C. G.; Yap, G. P. A.; Liable-Sands, L.; Rheingold, A. L.; Marchaj, A.; Norton, J. R. *J. Am. Chem. Soc.* **1997**, *119*, 1648.
(37) Shi, S.; Daniels, L. M.; Espenson, J. H. *Inorg. Chem.* **1991**, *30*, 3407.
(38) Lance, K. A.; Lin, W.-K.; Busch, D. H.; Alcock, N. W. *Acta Crystallogr.* **1991**, *C47*, 1401.
(39) Bakac, A.; Brynildson, M. E.; Espenson, J. H. *Inorg. Chem.* **1986**, *25*, 4108.
(40) Dreos, R.; Tauzher, G.; Vuano, S.; Asaro, F.; Pellizer, G.; Nardin, G.; Randaccio, L.; Geremia, S. *J. Organomet. Chem.* **1994**, *505*, 135.
(41) Asaro, F.; Dreos, R.; Geremia, S.; Nardin, G.; Pellizer, R., L.; Tauzher, G.; Vuano, S. *J. Organomet. Chem.* **1997**, *548*, 211.
(42) Fraser, B.; Brandt, L.; Stovall, W. K.; Kaesz, H.; Kahn, S. I.; Maury, F. *J. Organomet. Chem.* **1994**, *472*, 317.
(43) Jackman, M.; Klenk, M.; Fishburn, B.; Tullar, B. F.; Archer, S. *J. Am. Chem. Soc.* **1948**, *70*, 2884.
(44) Jönsson, Å. *Acta Chem. Scand.* **1954**, *8*, 1389.
(45) Hill, H. A. O.; Morallee, K. G. *J. Chem. Soc. A* **1969**, 554.
(46) Stewart, R. C.; Marzilli, L. G. *J. Am. Chem. Soc.* **1978**, *100*, 817.
(47) Brown, K. L. *J. Am. Chem. Soc.* **1979**, *101*, 6600.

Table 1. ^{1}H NMR Shift Data of Complexes (ppm)[a] in Acetone-d_6

L	Co−CH_3	oxime CH_3	L signals
		$LCo(DBF_2)_2CH_3$	
H_2O	1.02	2.34	
imH	1.21	2.37	7.64 (1H), 7.18 (1H), 6.81 (1H)
4-Me-imH	1.18	2.36	7.46 (1H), 6.46 (1H), 2.17 (3H)
4-*t*-Bu-imH	1.19	2.36	7.47 (1H), 6.47 (1H), 1.24 (9H)
		Dimer	
im^-	1.00	2.29	6.49 (1H), 6.21 (2H)
		$LCo(DH)_2CH_3$	
imH	1.21	2.38	7.65 (1H), 7.29 (1H), 6.80 (1H)
		Free Ligands	
imH			7.64 (1H), 7.05 (2H)
4-Me-imH			7.52 (1), 6.73 (1H), 2.11 (3H)
4-*t*-Bu-imH			7.51 (1H), 6.72 (1H), 1.28 (9H)

[a] Referenced to internal TMS.

Table 2. ^{1}H NMR Shift Data (ppm)[a] in Methanol-d_4

	Co−CH_3	oxime CH_3	L
		$LCo(DBF_2)_2CH_3$	
solvated	1.11	2.37	
imH	1.22	2.32	7.52 (1H), 7.07 (1H), 6.79 (1H)
4-Me-imH	1.19	2.31	7.34 (1H), 6.44 (1H), 2.16 (3H)
4-*t*-Bu-imH	1.21	2.32	7.39 (1H), 6.47 (1H), 1.23 (9H)
		Dimer	
im	0.99	2.27	6.51 (1H), 6.34 (2H)
		Free Ligands	
imH			7.68 (1H), 7.05 (2H)
4-Me-imH			7.52 (1H), 6.72 (1H), 2.20 (3H)

[a] Referenced to internal TMS.

the 18−19 ppm range also indicated replacement of the bridging H with BF_2. Without further purification, the complex was used to prepare the derivatives for this study.

$[H_2OCo((DO)(DOBF_2)pn)CH_3]PF_6$ was prepared from a suspension of $[H_2OCo((DO)(DOH)pn)CH_3]ClO_4$[48] (4.00 g, 9.29 mmol) in a 60:40 CH_2Cl_2/acetone mixture (330 mL). The suspension was purged with N_2 for 10 min before the addition of *n*-Bu_3N (3 mL), followed by a large excess of $BF_3{\cdot}Et_2O$ (18 mL). The cloudy suspension dissolved and was stirred overnight. Solvent was removed under reduced pressure to a volume of ∼50 mL, and Et_2O was added to precipitate $[H_2OCo((DO)(DOBF_2)pn)CH_3]ClO_4$ (4.39 g). The red solid was dissolved in hot H_2O (300 mL) and filtered into a hot, aqueous solution of KPF_6 (2.23 g in 50 mL). The solution was stored at 5 °C for several days, and the red crystals that formed were isolated by filtration and washed with Et_2O, yielding 2.22 g (4.24 mmol, 45.6%). ^{1}H NMR shift data are presented in Table 3. Anal. Calcd for $C_{12}H_{23}BCoF_8N_4O_3P$: C, 27.50; H, 4.43; N, 10.69. Found: C, 27.60; H, 4.45; N, 10.78.

$LCo(DBF_2)_2CH_3$ [L = imH (**1**), 4-methylimidazole (4-Me-imH)] was prepared by the addition of L (0.762 mmol) to an acetone solution of $H_2OCo(DBF_2)_2CH_3$ (0.3029 g, 0.725 mmol, in 20 mL). After the solution was stirred overnight, the solvent was removed under reduced pressure. Et_2O (20 mL) was added, and the suspension sonicated, filtered, and washed with a minimum of Et_2O. The solid was dried under vacuum overnight; yield of $imHCo(DBF_2)_2CH_3$ (**1**), 0.2830 g (0.605 mmol, 83.4%). Anal. Calcd for $C_{12}H_{19}B_2CoF_4N_6O_4$: C, 30.80; H, 4.10; N, 17.96. Found: C, 31.04; H, 4.16; N, 17.73. An orange crystal of **1** for X-ray diffraction was obtained by diffusing Et_2O into an acetone/benzene (∼80:20) solution of the complex. Yield of 4-Me-$imHCo(DBF_2)_2CH_3$ was 0.2761 g (0.5616 mmol, 85.9%). Anal. Calcd for $C_{13}H_{21}B_2CoF_4N_6O_4{\cdot}{}^1/_6(CH_3)_2CO$: C, 33.01; H, 4.51; N, 17.09. Found: C, 33.05; H, 4.42; N, 17.23.

$[AsPh_4][(\mu\text{-im})(Co(DBF_2)_2CH_3)_2]$ (**2**) was prepared by treating a methanol (30 mL) suspension of **1** (0.1598 g, 0.3415 mmol) with $NaOCH_3$ (0.17 g Na in 10 mL methanol). The suspension was stirred for 1 h and filtered to remove suspended solids. $[AsPh_4]Cl{\cdot}H_2O$ (0.30 g, 0.07 mmol) was added to the filtrate and refrigerated overnight. Yellow needles (0.1637 g, 0.1291 mmol, 80.79%) were isolated by filtration. Anal. Calcd for $C_{45}H_{53}AsB_4Co_2F_8N_{10}O_8{\cdot}H_2O$: C, 42.62; H, 4.37; N, 11.05. Found: C, 42.62; H, 4.18; N, 11.00. An orange crystal for X-ray structure determination was obtained by the diffusion of Et_2O into an acetone/benzene (∼80:20) solution of the complex.

4-*t*-Bu-$imHCo(DBF_2)_2CH_3$ (**3**) was prepared by adding 4-*t*-Bu-imH (0.11 g, 0.90 mmol) to a 70:30 acetone/$CHCl_3$ solution of $H_2OCo(DBF_2)_2CH_3$ (0.25 g, 0.60 mmol, in 28 mL). The mixture was refluxed gently overnight. After the solvent was removed under reduced pressure, the residue was dissolved in a minimum of $CHCl_3$, filtered, and placed in a freezer for 24 h. The solid product was isolated by filtration, dried under vacuum, and recrystallized from methanol to yield 0.21 g (0.40 mmol, 67%). Anal. Calcd for $C_{16}H_{27}B_2CoF_4N_6O_4{\cdot}{}^2/_3H_2O$: C, 35.85; H, 5.34; N, 15.68. Found: C, 36.13; H, 5.08; N, 15.42. An orange crystal was obtained for X-ray structure determination by cooling a concentrated methanol/ethyl acetate (60:40) solution of the complex.

$[imHCo((DO)(DOBF_2)pn)CH_3]PF_6$ (**4**) was prepared by the addition of imidazole (0.0428 g, 0.629 mmol) to a cloudy suspension of $[H_2OCo((DO)(DOBF_2)pn)CH_3]PF_6$ (0.2687 g, 0.513 mmol) in methanol (20 mL). A yellow solid precipitated almost immediately, and the mixture was stirred for another 15 min. The solid was isolated by filtration, washed with Et_2O, and dried under vacuum overnight, yielding 0.2063 g (0.359 mmol). Addition of Et_2O to the filtrate precipitated a second crop (0.0575 g, 0.100 mmol) for a total yield of 89.5%. Anal. Calcd for $C_{15}H_{25}BCoF_8N_6O_2P$: C, 31.37; H, 4.40; N, 14.64. Found: C, 31.43; H, 4.40; N, 14.59. An orange plate was obtained for X-ray structure determination by diffusing Et_2O into a concentrated acetone solution of the complex.

$[imHCo((DO)(DOH)pn)CH_3]PF_6$ was prepared by the addition of imidazole (0.08 g, 1.18 mmol) to a CH_2Cl_2 solution of $[H_2OCo((DO)(DOH)pn)CH_3]PF_6$ (0.3052 g, 0.641 mmol, in 20 mL). After stirring overnight, Et_2O was added until the solution became cloudy. The mixture was stored at 5 °C overnight. The yellow precipitate was isolated by filtration and dried under vacuum overnight to yield 0.3270 g of **5** (0.621 mmol, 96.9%). Anal. Calcd for $C_{15}H_{26}CoF_6N_6O_2P$: C, 34.28; H, 4.99; N, 15.97. Found: C, 34.29; H, 5.05; N, 15.93. A preparation of $[H_2OCo((DO)(DOH)pn)CH_3]PF_6$ containing residual iodide salts from the alkylation process was used in one synthesis of $[imHCo((DO)(DOH)pn)CH_3]PF_6$, which crystallized as $[imHCo((DO)(DOH)pn)CH_3]I$ (**5**) from the diffusion of Et_2O into an acetone/toluene (∼30:70) solution of the complex.

NMR Spectroscopy. ^{1}H 1D data collected on either a GE QE-300 or GN-600 Ω spectrometer were referenced to internal TMS. High-resolution one-bond proton−carbon coupling constants, $^1J_{CH}$ (±0.2 Hz), were obtained at 25 °C via the recently reported JHMQC (*J*-coupled heteronuclear multiple quantum coherence) method on the GN-600 Ω instrument.[29] Deprotonation studies of the imidazole complexes were performed in methanol-d_4 on saturated samples (∼2−5 mmol) using $NaOCD_3$ generated by the addition of Na to methanol-d_4.

X-ray Structural Determinations. All of the crystals were mounted under Paratone-8277 either on glass fibers or, if they were thin plates, in a loop, and immediately placed in a cold nitrogen stream at −80 or −90 °C on the X-ray diffractometer. The X-ray intensity data were collected on a standard Siemens SMART CCD area detector system equipped with a normal focus molybdenum-target X-ray tube operated at 2.0 kW (50 kV, 40 mA). Frames of data (1.3 hemispheres) were collected (total of 1321) using a narrow frame method with scan widths of 0.3° in ω and exposure times ranging from 30 s/frame using a detector-to-crystal distance of 5.09 cm (maximum 2θ angle of 56.54°) for all crystals except $imHCo(DBF_2)_2CH_3$ (**1**), for which a quadrant of data was collected using an exposure time of 10 s/frame. Frames were integrated with the Siemens SAINT program to 0.75 Å for all data sets except in the case of $[imHCo((DO)(DOH)pn)CH_3]I$ (**5**), for which data were integrated to 0.90 Å. Unit cell parameters for all of the crystals were based upon the least-squares refinement of three-dimensional centroids of >4000 reflections.[49] Data were corrected for absorption with the SADABS[50] program.

(48) Parker, W. O., Jr.; Zangrando, E.; Bresciani-Pahor, N.; Randaccio, L.; Marzilli, L. G. *Inorg. Chem.* **1986**, *25*, 3489.

Table 3. ^{1}H NMR Shift Data (ppm) for Imine/Oxime (I/O) $CoCH_3$ Complexes[a]

L	I/O	Co−CH_3	I/O CH_3	L signals
H_2O[b]	(DO)(DOBF$_2$)pn	1.12	2.61/2.44	
H_2O[c]	(DO)(DOBF$_2$)pn	1.08	2.49/2.41	
imH[b]	(DO)(DOBF$_2$)pn	1.14	2.68/2.49	7.57 (1H), 7.27 (1H), 6.58 (1H)
imH[c]	(DO)(DOBF$_2$)pn	1.11	2.53/2.43	7.34 (1H), 7.17 (1H), 6.46 (1H)
im dimer[c,d]	(DO)(DOBF$_2$)pn	0.96		6.35 (1H) 6.25 (2H)
imH[b]	(DO)(DOH)pn	0.76	2.55/2.34	7.55 (1H), 7.27 (1H), 6.62 (1H)

[a] Referenced to internal TMS, PF_6 salts. [b] Acetone-d_6. [c] Methanol-d_4. [d] Deuterium exchange complicates the spectrum of the equatorial methyl groups.

Table 4. Summary of Crystallographic Data for imHCo(DBF$_2$)$_2$CH$_3$ (**1**), [AsPh$_4$][(μ-im)(Co(DBF$_2$)$_2$CH$_3$)$_2$]·C$_6$H$_6$·(CH$_3$)$_2$CO (**2**), 4-*t*-BuimHCo(DBF$_2$)$_2$CH$_3$·CH$_3$OH (**3**), [imHCo((DO)(DOBF$_2$)pn)CH$_3$]PF$_6$ (**4**), and [imHCo((DO)(DOH)pn)CH$_3$]I (**5**)

	1	**2**	**3**	**4**	**5**
crystal parameters					
chemical formula	$C_{12}H_{19}B_2CoF_4N_6O_4$	$C_{54}H_{65}AsB_4Co_2F_8N_{10}O_9$	$C_{17}H_{27}B_2CoF_4N_6O_5$	$C_{15}H_{25}BCoF_8N_6O_2P$	$C_{15}H_{26}CoIN_6O_2$
fw	467.88	1386.18	552.00	574.12	508.25
cryst syst	orthorhombic	orthorhombic	orthorhombic	orthorhombic	orthorhombic
space group (no.)	*Pbca*	$P2_12_12_1$	$P2_12_12_1$	$Pca2_1$	$P2_12_12_1$
Z	8	4	4	8	4
a, Å	13.572	9.7279(1)	9.9133(1)	21.0109(1)	11.6554(1)
b, Å	15.7585(2)	24.0075(1)	15.2637(2)	7.5039(1)	12.5268(2)
c, Å	16.8442(1)	26.0171(1)	16.3786(2)	28.6043(4)	13.9249(2)
volume, Å^3	3602.54(5)	6076.10(7)	2478.31(5)	4509.86(9)	2033.10(5)
ρ_{calc}, mg mm^{-3}	1.725	1.515	1.479	1.601	1.660
cryst dimens, mm^3	0.26 × 0.28 × 0.34	0.26 × 0.28 × 0.30	0.12 × 0.20 × 0.24	0.08 × 0.18 × 0.20	0.16 × 0.18 × 0.26
temp, °C	−80	−80	−90	−80	−80
measurement of intensity data and refinement parameters[a]					
2θ range, deg	2.32−28.32	1.57−28.43	1.82−28.27	1.42−23.24	2.19−28.30
data collected	$-17 \le h \le 12$, $-19 \le k \le 18$, $-22 \le l \le 7$	$-11 \le h \le 12$, $-31 \le k \le 28$, $-28 \le l \le 34$	$-12 \le h \le 13$, $-17 \le k \le 19$, $-15 \le l \le 21$	$-16 \le h \le 28$, $-10 \le k \le 7$, $-37 \le l \le 36$	$-14 \le h \le 15$, $-11 \le k \le 16$, $-17 \le l \le 18$
no. of data collcd	11 350	37 902	15 508	17 912	12 525
no. of unique data	3921	14 530	5771	6245	4784
R_{int}, R_{sigma} (%)[b]	2.70, 3.20	3.53, 5.74	3.24, 4.54	4.07, 4.44	2.92, 4.06
no. of obs data ($I > 2\sigma(I)$)	3157	12 311	5103	5332	4197
no. of params varied	263	797	328	651	246
μ, mm^{-1}	1.027	1.174	0.762	0.924	2.383
range of transm factors	0.774−0.928	0.766−0.927	0.813−0.928	0.793−0.915	0.713−0.927
R1(F_o), wR2(F_2^o) obs (%)[c]	4.07, 8.45	4.59, 9.66	4.50, 10.90	4.71, 10.16	3.58, 7.37
R1(F_o), wR2(F_2^o) all (%)[c]	5.71, 9.08	5.89, 10.17	5.37, 11.48	5.80, 10.71	4.52, 7.76

[a] Radiation (λ, Å) = Mo Kα (0.710 73). Absorption correction = empirical (SADABS). [b] $R_{int} = \sum|F_o^2 - F_o^2(\text{mean})|/\sum[F_o^2]$; $R_{sigma} = \sum[\sigma(F_o^2)]/\sum[F_o^2]$. [c] $R1 = (\sum||F_o| - |F_c||)/\sum|F_o|$; $wR2 = [\sum[w(F_o^2 - F_c^2)^2]/\sum[w(F_o^2)^2]]^{1/2}$, where $w = 1/[\sigma(F_o^2) + (aP)^2 + bP]$ and $P = [(\text{Max};0,F_o^2) + 2F_c^2]/3$.

Space group assignments were made on the basis of systematic absences and intensity statistics by using the XPREP program.[51] The structures were solved by using direct methods and refined by full-matrix least-squares on F^2. For nearly all of the structures, the non-hydrogen atoms were refined with anisotropic thermal parameters, and hydrogens were generally included in idealized positions giving data/parameter ratios >10:1 (Supporting Information). There was nothing unusual about the solution or refinement of any of the structures, with the exception of [imHCo((DO)(DOBF$_2$)pn)CH$_3$]PF$_6$ (**4**). The space group for **4** was assigned as $Pca2_1$, which, for a *Z* value of 8, requires two independent molecules in the asymmetric unit. Upon close examination, no obvious extra crystallographic symmetry was detected, and the structure was refined as racemic twin. The O−BF$_2$−O ligand bound to Co(2) undergoes an orientational disorder with the oxygens and fluorines either above or below the Co(2)/B(12) vector; the SOF's (site occupation factors) of the disordered atom pairs refined to a 70:30 ratio. Further information, including the final residuals, from the X-ray diffraction studies appears in Table 4. Full experimental details, positional parameters for all atoms, anisotropic thermal parameters, all bond lengths and angles, and fixed hydrogen positional parameters are provided in the Supporting Information.

(49) The integration program SAINT has been noted to produce cell constant errors that are unreasonably small, since symmetric error is not included. More reasonable errors might be estimated at 10× the listed value.

(50) SADABS: The SADABS program is based on the method of Blessing; see: Blessing, R. H. *Acta Crystallogr. A* **1995**, *51*, 33.

(51) *SHELXTL: Structure Analysis Program*, version 5.04; Siemens Industrial Automation Inc.: Madison, WI, 1995.

Results

Structures. Selected geometric parameters for structures **1**−**5** and the one related published structure of a model with an endocyclic NH appear in Table 5. The ORTEP representations of the complexes are presented in Figures 1−5. Throughout the discussion, the neutral ligand atom numbering scheme will be that shown in Chart 2 to simplify comparison between analogous parts of the structures and to conform to the standard numbering scheme for Me_3Bzm in B_{12}-related complexes. In all five structures the Co atom was found at the center of a distorted octahedron, with the Co atom displaced toward the L group between 0.035 Å (**1**) and 0.055 Å (**3**) from the least-squares plane of the four equatorial N's. The hydrogen of the pyrrolic nitrogen of the imidazole in the structures of **1** and **3** displayed interactions with neighboring molecules. In **1**, N(6) was observed intermolecularly bonded to F(3) of an adjacent imHCo(DBF$_2$)$_2$CH$_3$; in the structure of **3**, the 2.876 Å distance between N(6) and the solvent O(1S) indicated a strong hydrogen bond.

(a) Equatorial Moiety. Since the BF_2 group does not lie in the equatorial plane, the replacement of the bridging proton with a BF_2 unit introduces an additional structural feature in the

Table 5. Selected Geometric Features of Imidazole-Containing MeB_{12} Model Complexes

	$(DH)_2$[a]	$(DBF_2)_2$[b]	I/O	I/O BF_2[c]	4-*t*-Bu-imH$(DBF_2)_2$[d]	μ-im dimer[e]
Co−N_L (Å)	2.019(3)	2.053(2)	2.032(3)	2.043(5)	2.054(3)	2.017(3)
				2.040(6)		2.018(3)
Co−C (Å)	1.985(3)	2.003(2)	1.991(5)	2.015(6)	2.002(4)	1.994(4)
				1.997(8)		1.988(4)
Co−N, av (Å)	1.880	1.866	1.893	1.886	1.866	1.857
				1.889		1.855
N_L−Co−C (deg)	177.2(12)	177.10(10)	179.5(2)	178.5(3)	179.4(2)	179.5(2)
				178.4(3)		179.3(2)
Co−N_L−C2 (deg)	129.7(12)	126.6(2)	127.3(3)	127.3(4)	127.9(2)	124.6(2)
				127.7(5)		124.6(2)
Co−N_L−C4 (deg)	124.8(12)	126.6(2)	126.9(3)	127.8(4)	127.0(2)	131.2(2)
				127.7(5)		130.8(2)
C2−N_L−C4 (deg)	105.3(3)	105.9(2)	105.8(4)	104.9(5)	105.1(3)	104.2(3)
				104.6(6)		104.6(3)
α (deg)	1.8	4.2	7.1	8.2	1.4	1.6
				4.1		1.0
d (Å)	0.029	0.035	0.052	0.051	0.055	0.038
				0.046		0.049
γ (deg)	85.1	76.7	88.9	89.6	88.4	88.4
				89.6		85.5
ϕ (deg)	1.7	40.0	74.2	67.9	46.6	48.97
				65.7		45.49

[a] Pattabhi, V.; Nethaji, M.; Gabe, E. J.; Lee, F. L.; Le Page, Y. *Acta Crystallogr. C* **1984**, *40*, 1155. [b] N(6) is H-bonded to F(3) of an adjacent $imHCo(DBF_2)_2CH_3$. [c] Top numbers are for one racemic twin; bottom numbers are for the other twin with 70/30 disorder. [d] There is a strong hydrogen bond between N(6) and the solvent O(1S) (2.876 Å). [e] Top numbers are for Co(1); bottom numbers are for Co(2).

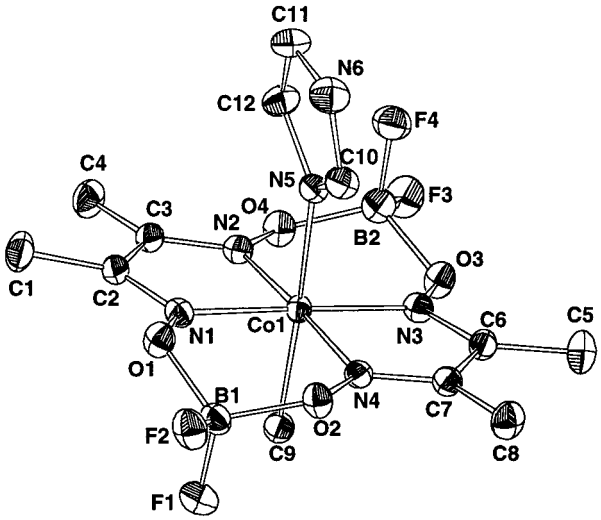

Figure 1. ORTEP drawing (thermal ellipsoid; 50% probability) for non-hydrogen atoms of **1**.

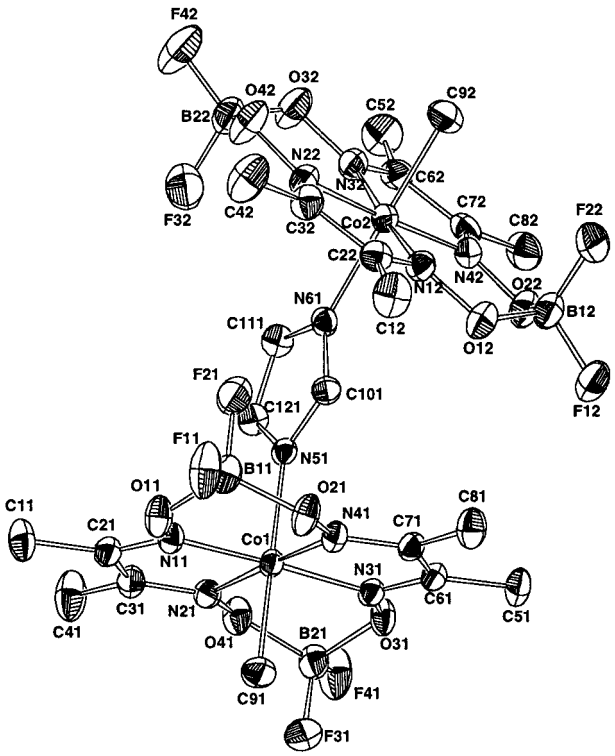

Figure 2. ORTEP drawing (thermal ellipsoid; 50% probability) for non-hydrogen atoms of **2**.

cobaloxime class of models. This feature, the orientation of the BF_2 unit relative to the equatorial plane (toward L or R), is similar to the displacement of the central moiety of the propanediyl (pn) bridge in I/O complexes. In complexes **1**−**3** and in the previously reported structures[36,38] of $LCo(DBF_2)_2CH_3$ (L = H_2O, Et_3P, py) and $(MeCN)Co(DBF_2)_2Cl$, the equatorial moieties adopt an extended chair conformation (Chart 3). In the I/O BF_2 complex, $[imHCo((DO)(DOBF_2)pn)CH_3]PF_6$ (**4**), the BF_2 group is oriented toward R, while the pn bridge is oriented toward L.

The dihedral angle (α) formed by the two equivalent halves of the dimethylglyoxime or I/O ligands quantifies the amount of butterfly bending in the equatorial moiety. In all cases, the butterfly bending is toward the axial methyl group (assigned a positive α value) (Table 5).

(b) Axial Coordination. The Co−C bond distances increase in response to BF_2 substitution in the cobaloximes very slightly, and there is no significant change for the I/O complexes. Changes in the Co−L metric parameters can be understood on the basis of L orientation (cf. next paragraph). The Co−N_L bond distance in the cobaloxime system increased significantly from ~2.02 to ~2.05 Å when BF_2 was substituted for the bridging protons. The same comparison in the I/O system does not show a significant increase. The angles involving the coordinated axial nitrogen atom, N_L, have been used in describing the steric requirements of coordinated Me_3Bzm and other alkylated imidazole derivatives.[20,25,30] Following BF_2 substitution, the imH in the cobaloxime complex tilts by ~3° with respect to the Co−N_L axis, thereby increasing the Co−N_L−C2 angle and decreasing the Co−N_L−C4 angle. The analogous imH I/O

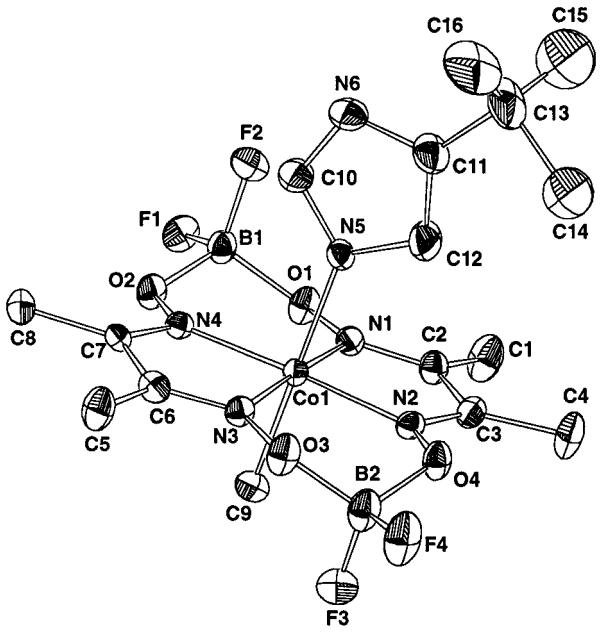

Figure 3. ORTEP drawing (thermal ellipsoid; 50% probability) for non-hydrogen atoms of **3**.

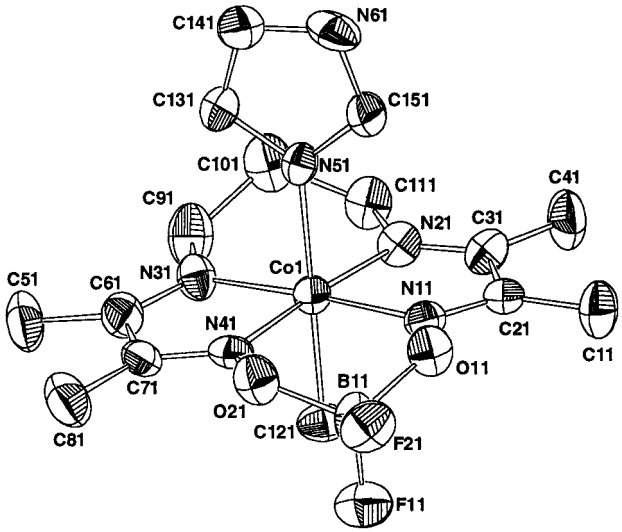

Figure 4. ORTEP drawing (thermal ellipsoid; 50% probability) for non-hydrogen atoms of **4**.

system shows no significant change in these angles between the BF_2 and non-BF_2 complexes.

(c) Orientation of the L Plane. Cobaloximes and I/O's are known to exhibit characteristic orientations of planar L ligands with respect to the O−H- - -O bridging unit. Standard I/O structures exhibit the B-type orientation (Chart 4) exclusively, whereas cobaloxime structures show the A-type orientation with only three exceptions.[30] The distinction between the two orientations has been quantified by the ϕ angle, defined as the torsion angle N*−Co−N_L−C2, where N* is the midpoint of the vector between the N's of the bridging O−X−O unit. When viewed from the L side of the complex, ϕ is assigned a negative value for a counterclockwise rotation around the Co−N_L bond. The A orientation of cobaloximes has a typical $|\phi|$ range of 0−23° when L = Me_3Bzm, whereas Me_3Bzm-containing I/O's display a range of $|\phi|$ values of 57−119°.[20,25] The values found here for the I/O complexes are typical (Table 5). In the BF_2 cobaloximes (**1**−**3**), the $|\phi|$ angles range from 40° to 49°, or

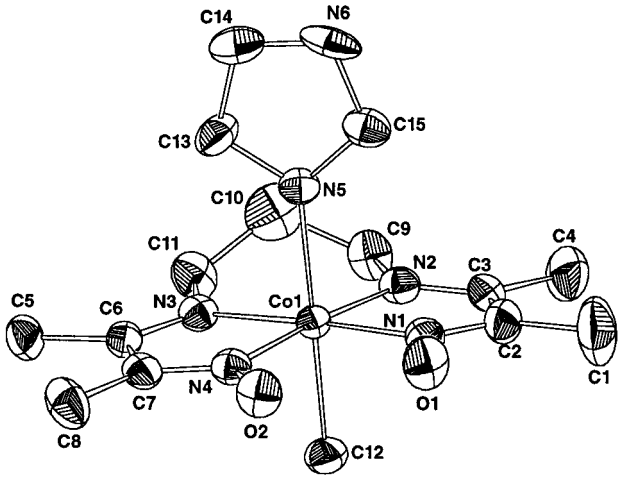

Figure 5. ORTEP drawing (thermal ellipsoid; 50% probability) for non-hydrogen atoms of **5**.

Chart 2

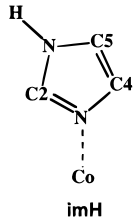

imH

Chart 3

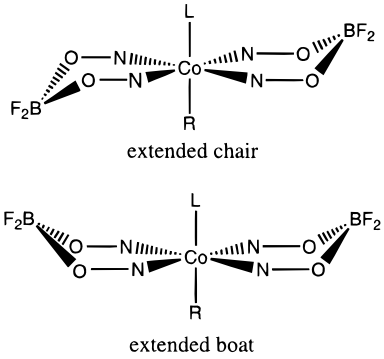

extended chair

extended boat

Chart 4

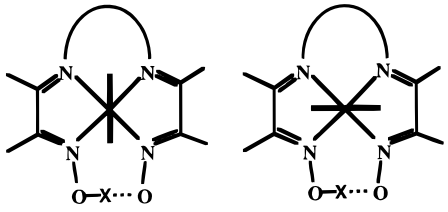

= –O—X–O– (cobaloxime), $-CH_2CH_2CH_2-$ (I/O)

X = H, BF_2

approximately halfway between A and B type orientations. The structure reported for $pyCo(DBF_2)_2CH_3$ exhibited a B-type orientation[36] with ϕ = 89°. This difference between a six-membered ring L (py) and the five-membered ring L compounds is consistent with the smaller steric bulk of the five-membered ring systems.

The orientation of the L plane has also been characterized in terms of the γ angle, defined as the angle between the least

squares planes of the four equatorial N's and the plane of the L group. In all of our structures except imHCo(DBF_2)$_2CH_3$ (**1**, Table 5), the γ angle had a value ~90°.

(d) Dimer Features. The two halves of the μ-imidazolato-bridged dimer (**2**) display some differences from the structure of imHCo(DBF_2)$_2CH_3$ (**1**). The Co−N_L distances are significantly shorter than that of the imidazole BF_2 monomer and resemble that of imHCo(DH)$_2CH_3$; however, the Co−C bond distances are comparable to those of the imHCo(DBF_2)$_2CH_3$ and imHCo(DH)$_2CH_3$ complexes. The C−Co−N_L angles are close to 180° in both the dimer and the imidazole monomer. The most striking difference between **1** and the dimer (**2**) is the relative value of the Co−N_L−C angles (Table 5), which are less symmetric in the dimer, with values typical of Me_3Bzm complexes. The dihedral angle between the planes defined by the four equatorial N's of each half of **2** is 135.4°. The equatorial moieties in each half adopt an extended chair conformation (Chart 3). Viewed down the Co(1)−Co(2) vector, the two halves are oriented such that the BF_2 units are ~90° apart, resulting in a ϕ value that is halfway between the A and B orientations of L.

NMR Studies in Acetone-d_6. ^{1}H NMR data (Tables 1 and 3) for comparison between BF_2 and non-BF_2 complexes were acquired in acetone-d_6 for solubility reasons. The oxime methyl, imine methyl (for I/O's), and Co−CH_3 signals show the largest change, moving downfield in response to the substitution of H with BF_2. These signals in the μ-imidazolato complex (**2**) lie upfield of the monomer complex (**1**). In both acetone-d_6 and methanol-d_4, the Co−CH_3 signals of the BF_2 cobaloximes appear as triplets with 1−2 Hz separation, consistent with long-range coupling to ^{19}F.[52]

The L group shifts also reveal some trends in response to BF_2 substitution. In the imidazole complexes, the ^{1}H signals closest to the site of coordination (CH2, CH4) move downfield, while the CH5 signal moves upfield. These changes are less pronounced in the I/O complexes with respect to the cobaloximes. In the dimer, the imidazole signals all shift upfield by >0.5 ppm.

NMR Studies in Methanol-d_4. Despite the limited solubility (2−4 mM) of **1** in methanol-d_4, we used this solvent in attempts to generate imidazolate complexes since sodium methoxide is a convenient strong base. An analytically pure sample (having the correct ^{1}H NMR spectrum in acetone-d_6) of imHCo(DBF_2)$_2$-CH_3 (**1**) has an initial CD_3OD spectrum with an extra set of oxime methyl and Co−CH_3 signals (2.37 and 1.11 ppm, respectively) approximately one-third as intense as the main signals (2.32 and 1.22 ppm, Figure 6). Only one set of three sharp coordinated imidazole signals (1:1:1) was clearly observable (7.52, 7.07, and 6.79 ppm, Figure 7). However, two broad signals were noted at ~7.70 and ~7.08 ppm, corresponding roughly to free imidazole. The extra set of methyl signals is assigned to the solvated (methanol) complex.

After the addition of a small amount of $NaOCD_3$, the initial coordinated imidazole signals disappeared almost completely (Figure 7). Two roughly equal sets of two aromatic signals in a 1:2 ratio (7.67, 7.05 ppm and 6.52, 6.34 ppm) eventually appeared. The downfield set is from free imidazole. Only one set of signals for the oxime methyl (2.28 ppm) and Co−CH_3 (0.99 ppm, Figure 6) groups was found. The formation of a dimer explains these results. The dimer was isolated and structurally characterized as [$AsPh_4$][(μ-im)(Co(DBF_2)$_2CH_3$)$_2$] (**2**). The ^{1}H NMR spectrum of the salt in methanol confirmed

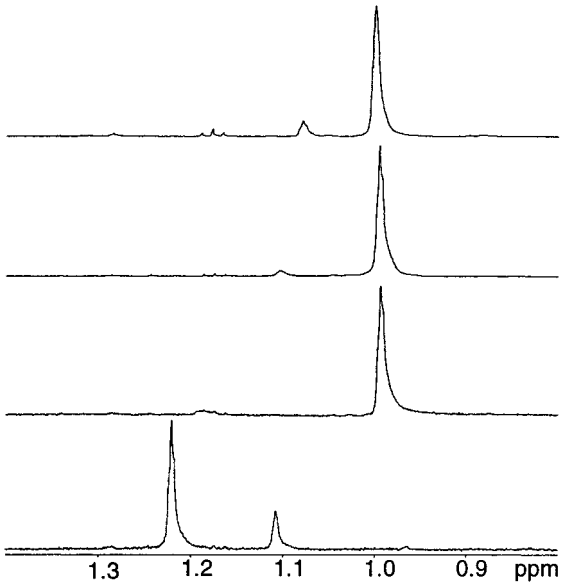

Figure 6. Co−CH_3 region of ^{1}H NMR spectra of the titration of **1** in CD_3OD. Bottom to top: 0, 0.5, 2, and 15 total molar equiv of $NaOCD_3$ added.

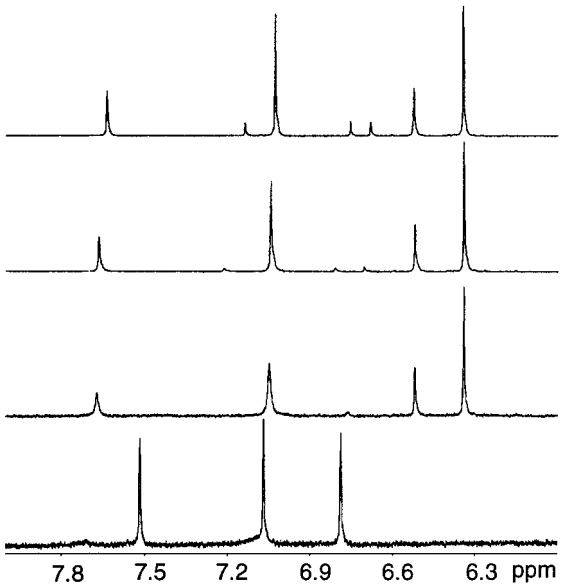

Figure 7. Aromatic region of ^{1}H NMR spectra of the titration of **1** in CD_3OD. Bottom to top: 0, 0.5, 2, and 15 total molar equiv of $NaOCD_3$ added.

that the signals following the additions of $NaOCD_3$ belong to the dimer.

When more $NaOCD_3$ was added, a new set of three signals in a 1:1:1 ratio (7.21, 6.81, and 6.70 ppm, Figure 7) for coordinated imidazole and a second Co−CH_3 signal (1.09 ppm, Figure 6) appeared. When the amount of base was increased even further, the relative integral of these new signals increased slightly. The new set of three singlets suggests formation of the desired monomeric imidazolato complex; however, we were unable to shift the equilibrium to favor complete conversion of the mixture to the imidazolato-bound complex. The oxime methyl signals provided little information over the course of the experiment since these protons exchanged for deuterium.

In the similar titration of [imHCo((DO)($DOBF_2$)pn)CH_3]PF_6 (**4**, Supporting Information), the initial spectrum contained a set of three aromatic peaks in a 1:1:1 ratio, indicating the dominance of the intact imidazole complex. Free imidazole

(52) Jameson, C. J. In *Multinuclear NMR*; Mason, J., Ed.; Plenum Press: New York, 1987; p 437.

signals were present, along with a third set of signals (6.35, 6.25 ppm in a 1:2 ratio), almost indistinguishable from the baseline and suggesting the presence of a small amount of the imidazolato dimer. The Co−CH_3 region also displayed two minor signals (1.09 and 0.96 ppm); the former corresponds to the Co−CH_3 shift for $[H_2OCo((DO)(DOBF_2)pn)CH_3]PF_6$ in methanol and indicates a solvated complex. Addition of $NaOCD_3$ led to an increase in the intensity of all the signals for free imidazole and the dimer at the expense of the signals of the intact complex. In this case, the dimer had signals in the expected ratio (Table 3) but it could not be isolated. Furthermore, as found for $[AsPh_4][(\mu\text{-im})(Co(DBF_2)_2CH_3)_2]$ (**2**), the aromatic and Co−CH_3 signals were shifted upfield with respect to the parent imidazole complex.

In an effort to hinder sterically the formation of the μ-imidazolato dimer, 4-substituted imidazole derivatives, namely, 4-Me-im$HCo(DBF_2)_2CH_3$ and 4-*t*-Bu-im$HCo(DBF_2)_2CH_3$ (**3**), were prepared. Samples of both complexes in CD_3OD display two sets of aromatic signals in the initial ^{1}H NMR spectrum, consistent with solvation. However, addition of base or allowing the samples to stand led to signal patterns different from those for the nonsubstituted imidazole complexes (not shown). Neither the 4-Me-imH nor the 4-*t*-Bu-imH product could be isolated.

JHMQC Studies. The JHMQC method was utilized to determine $^1J_{CH}$ values for the imidazole-containing cobaloxime complexes with and without the BF_2 substitution. Acetone-d_6 solutions were used since this was the only solvent giving an adequate concentration of all the complexes without displacing imidazole, as found for coordinating solvents such as DMSO. The im$HCo(DBF_2)_2CH_3$ (**1**) complex has $^1J_{CH}$ values for the oxime methyl and Co−CH_3 groups of 130.9 and 140.5 Hz, respectively, greater than those of the im$HCo(DH)_2CH_3$ (129.4 and 135.9 Hz, respectively). Values for the oxime methyl and Co−CH_3 groups in $[AsPh_4][(\mu\text{-im})(Co(DBF_2)_2CH_3)_2]$ (**2**) are 130.8 and 138.4 Hz, respectively.

Discussion

Structures. In general, the equatorial moiety of the $(DH)_2$ cobaloximes is relatively planar, with small α values leading to the predominance of the A orientation of L (Chart 4). On the other hand, py$Co(DBF_2)_2CH_3$ has a relatively large α ($\sim$7°) and the py has adopted a B-orientation ($\phi = 89°$).[36] The increase in α demonstrates butterfly bending toward the methyl group following BF_2 substitution; this bending provided more space on the py face of the equatorial plane for py to adopt the B orientation, which is rarely observed for $(DH)_2$ cobaloximes. In fact, *N*-methylimidazole is the only ligand to adopt the B orientation in the $(DH)_2$ cobaloximes, but only when butterfly bending toward the R group prevents unfavorable steric interactions between L and the equatorial plane.[30] Furthermore, the substitution of H by BF_2 groups in the bridging unit produces puckered chelate rings, which lie either above or below the equatorial plane (Chart 3); this puckering is similar to that of the pn bridge of I/O complexes. Steric interactions between the pn bridge of I/O complexes and L lead to the B orientation in the I/O class of models (Chart 4).[6,16,25,33] A similar steric effect was attributed to the BF_2 groups in order to explain the B-orientation of py in py$Co(DBF_2)_2CH_3$[36] (see also refs 40 and 41). The equatorial ligands in all L$Co(DBF_2)_2CH_3$ species have an extended chair conformation (Chart 3), which forces the axial ligand out of the pure A-type orientation normally observed. The $(DBF_2)_2$ cobaloximes presented here, including the dimer (**2**), exhibit an axial ligand orientation approximately halfway between the A- and B-type structures. The Co−N_L distance is significantly longer in im$HCo(DBF_2)_2CH_3$ (**1**) than in im$HCo(DH)_2CH_3$, establishing that steric effects are significant. Thus, additional evidence for this steric effect in $(DBF_2)_2$ cobaloximes was found here. However, the five-membered ring imH, 4-*t*-Bu-imH, and im ligands are apparently small enough to be able to adopt the intermediate A/B-type orientation.

For the I/O system, the effect of BF_2 substitution on L orientation is more difficult to assess since the pn bridge already dictates the B orientation in $[imHCo((DO)(DOH)pn)CH_3]I$. In $[imHCo((DO)(DOBF_2)pn)CH_3]PF_6$ (**4**), the extended chair conformation of the pn and BF_2 bridging units is anticipated from the conformation observed in the cobaloximes. The BF_2 groups in cobaloximes have been reported to equilibrate on the NMR time scale between the extended chair and extended boat conformations in solution, and the observation of only the extended chair conformation in the solid state has been attributed to solid-state effects.[36]

In $[AsPh_4][(\mu\text{-im})(Co(DBF_2)_2CH_3)_2]$ (**2**), the imidazolato ligand adopts the staggered orientation with respect to both of the monomeric units of **2**. The imidazolato orientation is halfway between the A and B types; this intermediate orientation, which minimizes steric interactions with both halves of the dimer, is the same orientation as found for the monomer, im$HCo(DBF_2)_2CH_3$. Thus, the significantly shorter Co−N(imidazolato) bond length relative to the Co−N(imidazole) bond length (Table 5) most probably reflects the greater electron-donating ability of the imidazolato ligand. The structural observations are consistent with previous observations on the effects of the A → B orientation on Co−N(L) bond lengths.[6,13,30,33]

NMR Spectroscopy. Interpretation of the changes in the ^{1}H NMR shifts resulting from BF_2 substitution is difficult since inductive, anisotropic, and steric effects all contribute to the observed shift. However, the $^1J_{CH}$ values for the Co−CH_3 moiety in the imidazole complexes provide insight into the effect of BF_2 on the metal center. Quantitatively, this change can be expressed as ρ_{CH} (the percent s character in the C hybrid orbital) using the relationship $^1J_{CH}$ (Hz) = $500\rho_{CH}$.[53] Thus, the observed increase in $^1J_{CH}$ for the Co−CH_3 moiety accompanying BF_2 substitution indicates an increase in s character from 27.2% to 28.1%. For comparison, the change in Co−CH_3 $^1J_{CH}$ values in L$Co(DH)_2CH_3$ resulting from variation of L through a series of phosphines indicated an increase in the s character of the C hybrid orbitals from 27.4% to 28.1% as the pK_a of the P-donor decreased from 9.70 (tricyclohexylphosphine, Cy_3P) to 1.03 ($(p\text{-ClPh})_3P$).[31] According to Bent's Rule,[54] the increase in s character of the C hybrid orbital in the CH bond and the corresponding decrease in s character of the C hybrid orbitals in the Co−C bond reflect an increase in the electronegativity of the Co atom accompanying BF_2 substitution. Clearly the substitution of the bridging H's with BF_2 moieties results in an increase in the electronegativity of Co similar in magnitude to that observed for very large changes in L from the more σ-donating Cy_3P to the less σ-donating $(p\text{-ClPh})_3P$.[31] However, the effect is not large. The $^1J_{CH}$ value of the Co−CH_3 moiety of $[AsPh_4][(\mu\text{-im})(Co(DBF_2)_2CH_3)_2]$ (**2**) indicates a reduction in the s character of the C hybrid orbital to 27.7%. This reduction is expected since the μ-imidazolato ligand is more electron-donating than imidazole and counteracts, in part, the effect of the BF_2 bridges.

There are pronounced upfield shifts of the aromatic signals on dimer formation. These shifts are consistent with the expected

(53) Drago, R. S. In *Physical Methods for Chemists*, 2nd ed.; Saunders College Publishing: New York, 1992.
(54) Bent, H. A. *Chem. Rev.* **1961**, *61*, 275.

Chart 5

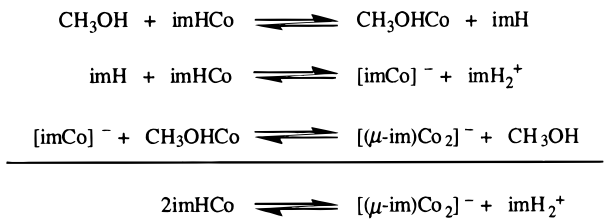

increase in electron density in the imidazole ring upon formation of an imidazolato ligand.

Dimer Formation. The small extra sets of imidazole signals in the initial spectra of analytically pure imHCo(DBF_2)$_2$$CH_3$ (**1**), 4-*t*-Bu-imHCo(DBF_2)$_2$$CH_3$ (**3**), [imHCo((DO)($DOBF_2$)pn)-CH_3]PF_6 (**4**), and 4-Me-imHCo(DBF_2)$_2$$CH_3$ suggest partial solvation by methanol. Evidence for dimers was obtained for **1** and **4**. We propose the scheme in Chart 5 to explain the dimerization process for **1** and **4**. Given the presence of characteristic protonated imidazole signals in the spectrum over time and the observation that dimerization does not occur in the weakly coordinating solvent acetone-d_6, it seems likely that partial displacement of the bound imidazole by methanol is a key initial step. The displaced imidazole is a base and partially deprotonates bound imidazole to generate a transient imidazolato complex and an imidazolium ion. The imidazolato complex then forms the dimer in a subsequent reaction with the methanol complex. As the imidazoles and solvated species are consumed through protonation and dimer formation, the imidazole monomer dissociates, replenishing these species. This process is greatly accelerated by the addition of methoxide.

Conclusions

We have greatly increased the number of structurally and spectroscopically characterized imidazole-containing B_{12} models with an imidazole endocyclic NH group. Recent evidence shows such axial ligation occurs in many B_{12} enzymes. Hydrogen bonding by the NH group could modulate the imidazole binding. The generation of imidazolato ligands under basic conditions is one way to probe the possible limits of such modulation. The substitution of BF_2 groups into the bridging unit of standard B_{12} model complexes has been shown to be a reasonable approach to studying such models under basic conditions. However, the imidazolato monomers proved to be less favored than the μ-imidazolato-bridged dimers. Such dimers are perhaps more interesting than the initally targeted monomers since the bridged imidazolato moiety is a closer analogue of an imidazole donating a strong H-bond than is the monodentate imidazolato moiety. We found with NMR coupling constant data that the μ-imidazolato moiety was electron-donating enough to produce a change in the s character of the CH bond of the Co−CH_3 moiety; this change is comparable to that observed for Co−CH_3 complexes with an extensive range of trans axial ligand with increasing σ-donating abilities. The NMR data indicate that BF_2-substitution makes the Co center more electronegative. The Co−N(imidazolato) bond length is shorter than the Co−N(imidazole) bond length, but there are no significant changes in the trans Co−C bond lengths.

Acknowledgment. This work was supported by NIH Grants GM 29225 and GM 29222 (to L.G.M.).

Supporting Information Available: Tables of bond lengths and angles, hydrogen atom coordinates, and anisotropic thermal parameters and ^{1}H NMR spectra of [ImdCo((DO)($DOBF_2$)pn)CH_3]PF_6 in methanol-d_6. This material is available free of charge via the Internet at http://pubs.acs.org.

IC980944D